



# Fabrication of 2D nanomaterial reinforced co-continuous binary blend composites for thermal management and EMI shielding applications

Ankur Katheria<sup>1</sup> · Palash Das<sup>1</sup> · Suman Kumar Ghosh<sup>1</sup> · Jasomati Nayak<sup>1</sup> · Krishnendu Nath<sup>1</sup> · Sangit Paul<sup>1</sup> · Shovan Biswas<sup>1</sup> · Narayan Ch. Das<sup>1</sup>

Received: 10 September 2023 / Accepted: 27 November 2023 / Published online: 2 December 2023  
© The Polymer Society, Taipei 2023

## Abstract

Polymer nanocomposites have garnered significant interest for electromagnetic interference (EMI) shielding applications due to their lightweight, anticorrosive and tunable properties. Employing the solution blending technique, we have developed a composite material comprising an 80wt% EMA (Ethylene–Methyl Acrylate) and 20wt% TPO (Thermoplastic Polyolefin) co-continuous blend. The incorporation of Reduced Graphene Oxide (RGO) as a conductive filler is achieved through precise confinement within the EMA phase of the polymer matrix. The selective placement of the RGO nanosheets within the EMA phase results in a dual percolation phenomenon, significantly lowering the electrical percolation threshold. A notable EMI SE value of -29.66 dB and electrical conductivity of  $10^{-3}$  S/cm is achieved with the addition of 5wt% RGO. Further optimizing the composite, a loading of 15wt% RGO showcases an outstanding EMI SE of -39.06 dB. Moreover, this composite demonstrates commendable thermal conductivity of 0.75 W/m.K, alongside promising mechanical properties. The findings offer a promising avenue for the integration of this material in EMI-sensitive applications, particularly in the realms of stretchable and wearable electronics, offering effective thermal management and proficient microwave shielding capabilities.

**Keywords** Thermoplastic polyolefin · Ethylene-co-methyl acrylate · Reduced graphene oxide · Thermal conductivity · EMI shielding effectiveness · Dielectric constant

## Introduction

In light of the rapid expansion of the modern electronic industry, particularly with the advent of the 5G network era, electronic devices and wireless communication technologies have witnessed extensive integration into various applications. The ease of communication that technology provides has raised concerns regarding electromagnetic interference (EMI) and its consequential effects on electromagnetic pollution. The impact of electromagnetic (EM) waves extends beyond the impairment of technological and communication devices; it poses a lasting and profoundly adverse threat to human health. Consequently, the crucial arises to address the challenge of EM pollution with effective and viable strategies. EMI shielding has emerged as the practical and efficient approach to counter EM pollution [1–5]. To

diminish EM waves at its source, EMI shielding materials are commonly employed to hinder the propagation of EM waves, achieved through reflection or containment within the shielding structure. Although metals have historically been the chosen option for electromagnetic interference (EMI) shielding because of their exceptional electrical conductivity, they also possess certain disadvantages. Notable among these are high density, inflexibility, manufacturing complexities, susceptibility to corrosion [6–9].

Certain widely known conductive polymers, such as polypyrrole and polyaniline, face challenges in gaining widespread acceptance due to their deficient design and limited conductivity [10]. The demand for a lightweight electromagnetic interference (EMI) shielding material has prompted the need for meticulous design. In the contemporary landscape, polymer-based composites have garnered significant attention as a viable alternative to conventional metal-based materials for effective EMI shielding. This shift can be attributed to their inherent attributes, including lightness, resistance to corrosion, ease of processing, and potential for reuse [11–14]. These attributes have led

✉ Narayan Ch. Das  
ncdas@rtc.iitkgp.ac.in

<sup>1</sup> Rubber Technology Centre, Indian Institute of Technology, Kharagpur 721302, West Bengal, India

to the propagation of their use in efficient EMI shielding applications. While polymeric matrices are typically considered electrically insulating and susceptible to electromagnetic radiation, their amalgamation with conductive additives results in the emergence of an efficient EMI shielding material, facilitated by the formation of a conductive path within a matrix. Carbonaceous additives have gained prominence as conductive fillers due to their intrinsic conductivity. Materials like carbon black, graphene nanoplatelets, carbon nanotube (CNT), carbon nanofibers (CNFs), have exhibited remarkable EMI shielding capabilities.

For example, the authors Poushali et al. discussed the fabrication process and EMI SE of nanocomposites made from EMA and in-situ reduced graphene oxide (IRGO) fillers. It is worth mentioning that a maximum electromagnetic interference (EMI) shielding effectiveness (SE) of 34.9 dB was attained when utilising a filler loading of 7 wt% in the X-band frequency range. The composite materials exhibited an increasing electromagnetic interference shielding effectiveness, which can be attributed to the absorption mechanism assisted by densely packed network topologies [15]. Arunima et al. innovatively fabricated a hybrid composite with high EMI shielding efficiency, incorporating discarded cigarette wrapper (CW) within a composite matrix of PDMS and RGO. Remarkably, an overall shielding efficiency of 50.79 dB was recorded in the 14.5–20 GHz range [16]. Furthermore, Meng et al. documented the development of DGEBA/PEI/RGO ternary nanocomposites through solution blending. Impressively, a substantial EMI SE of 25.8 dB was observed in the 8.2–12.4 frequency range with just 3 wt% RGO loading [17].

The concept of the "percolation threshold" holds significant importance in the formulation of conductive polymer composites. It denotes the critical concentration of filler at which an insulator transitions into a conductor. This threshold is influenced by various factors, including filler type, its dispersion, and the composite preparation conditions. Lowering the percolation threshold stands as an efficient strategy for cost savings and improved composite processability. Diverse techniques, filler modification [18], hybrid filler utilisation [19], in-situ polymerisation of monomers with filler, and novel compounding approaches, have been devised to enhance electrical conductivity and percolation threshold. Particularly effective is the method of reducing the percolation threshold through the incorporation of filler, especially particle-based carbonaceous fillers, within a co-continuous immiscible polymer blend matrix. This approach establishes a dual-percolation continuous conductive path across the polymer matrix by selectively positioning the filler in one phase of the binary co-continuous polymer blends.

However, while enhancing electrical conductivity in polymer composites is advantageous, it poses challenges for electromagnetic interference shielding effectiveness (EMI

SE) in wearable and portable electronics. This is due to the necessity of considering the material's thermal conductivity. EMI shielding materials absorb electromagnetic radiation, generating substantial heat energy that can adversely affect device performance and lifespan. Therefore, this study presents EMA/TPO/RGO polymer blend composites that offer both impressive thermal conductivity and flexibility, alongside efficient EMI SE.

The surface of reduced graphene oxide (RGO) is known for its high concentration of functional groups and defects. These features promote the relaxation of dipoles and the polarisation of defects, resulting in an increased absorption of outgoing electromagnetic radiation [20]. In addition to possessing robust mechanical properties and low-temperature flexibility, the copolymer poly(ethylene-co-methyl acrylate) (EMA) features both polar (acrylic) and non-polar (ethylene) domains, granting it excellent weather resistance, thermal stability, and resistance to ageing. On the other hand, the thermoplastic polyolefin (TPO), namely Tafmer DF 740, is classified as an elastomer derived from ethylene-based alpha-olefin. This material is highly regarded for its notable characteristics such as elasticity, transparency, and exceptional resistance to impact, particularly in low-temperature environments. The chosen blend system, EMA/TPO (80/20), exhibits outstanding qualities including remarkable weather resistance, impressive impact resistance at lower temperatures, flexibility, heat resistance, and enduring lasting strength with repeated use. Moreover, the immiscibility of this blend results in a co-continuous morphology. This unique morphology facilitates the preferential distribution of conductive RGO filler in one phase of the polymer blend, allowing for reduced filler concentrations while achieving optimal electrical and thermal conductivity. As a result, the newly developed EMI shielding composite is produced in a straightforward and economical manner, positioning it as a promising and effective substitute for traditional EMI shielding materials in the realm of flexible and intelligent electronics applications.

## Experimental

### Materials

The polymer Elvaloy® 1330, which falls under the category of poly(ethylene methyl acrylate) (EMA), has been obtained from DuPont India Pvt. Ltd. located in Mumbai. It has a molecular weight of 186,000 g/mol (Mw), a melt flow index (MFI) of 3.0 g per 10 min (according to ASTM D1238), and consists of 30% methyl acrylate. The thermoplastic olefin (TPO) utilised in the investigation was procured from Mitsui Chemicals Singapore under the brand name Tafmer DF 740. It possessed a molecular weight of 330,000 g/mol (Mw). The reduced technique was utilised in our laboratory

to synthesise reduced graphene oxide (RGO). The necessary materials for the experiment, such as natural graphite flakes, hydrazine ( $\text{N}_2\text{H}_4$ , 35%), hydrochloric acid (HCl), and hydrogen peroxide ( $\text{H}_2\text{O}_2$ , 30%), were provided by Loba Chemie Pvt. Ltd. Furthermore, the following chemicals were obtained from Merck India: Chloroform ( $\text{CHCl}_3$ ), sulphuric acid ( $\text{H}_2\text{SO}_4$ , 95%), phosphoric acid ( $\text{H}_3\text{PO}_4$ , 85%), and potassium permanganate ( $\text{KMnO}_4$ ). The laboratory-based reduction technique was employed in the manufacture of reduced graphene oxide (RGO).

### Synthesis of GO and RGO

The production of graphene oxide (GO) was conducted using the Modified Hummer technique, commencing with the utilisation of finely powdered graphite [16]. A mixture of 40 mL of  $\text{H}_3\text{PO}_4$  and 360 mL of concentrated  $\text{H}_2\text{SO}_4$  acid was combined with 3.0 g of graphite powder and subsequently agitated. During the process of stirring, the solid compound  $\text{KMnO}_4$  was progressively added to the acidic solution. After undergoing continuous stirring for a duration of 12 h, the mixture was subjected to an infusion of 500 mL of cold water. Subsequently, a gradual addition of  $\text{H}_2\text{O}_2$  was initiated until the mixture exhibited a pale yellow colour. After a period of 30 min of continuous stirring, the solution was afterwards allowed to remain undisturbed for a duration of three days. The resulting brown precipitate (GO) was carefully rinsed with distilled water for a duration of three days in order to remove any residual salts and acids

thoroughly. Subsequently, the material underwent a drying process in a hot air oven in order to remove any moisture that may have been trapped within.

Reduced graphene oxide (RGO) was prepared from graphene oxide (GO) by adding GO powder to a flask containing purified water ( $3 \text{ mg mL}^{-1}$ ). Hydrazine monohydrate ( $1 \mu\text{L}$  for 3 mg of GO) was then immediately added, and the mixture was stirred for 12 h at  $80^\circ\text{C}$  in an oil bath. For later usage, the black precipitate of RGO that resulted was filtered out and dried in a hot air oven.

### Fabrication process of EMA/TPO/RGO composite

The process of fabricating a composite consisting of an EMA/TPO/RGO is demonstrated in Fig. 1, employing magnetic stirring, predetermined quantities of EMA and TPO were dissolved in a solvent. After full dissolution, the solutions were homogenised through a 1-h blending process. Prior to addition to the polymer blend, RGO underwent ultrasonic treatment for 1 h. The homogenised polymer blend solution received RGO drop wise, followed by a 1.5-h stirring period. The resulting solution was poured into a Petri dish and left undisturbed for a duration of 24 h to facilitate the evaporation of the solvent. The dried composite was subsequently shaped into a 1 mm sheet utilising a hot press compression moulding machine for 5 min under a pressure of 5 MPa. The resultant nanocomposites were labelled as  $\text{E}_x\text{T}_x\text{R}_x$ , where  $\text{E}_x$  signifies the EMA weight percentage,  $\text{T}_x$  denotes the TPO weight percentage, and  $\text{R}_x$  represents the RGO weight percentage.

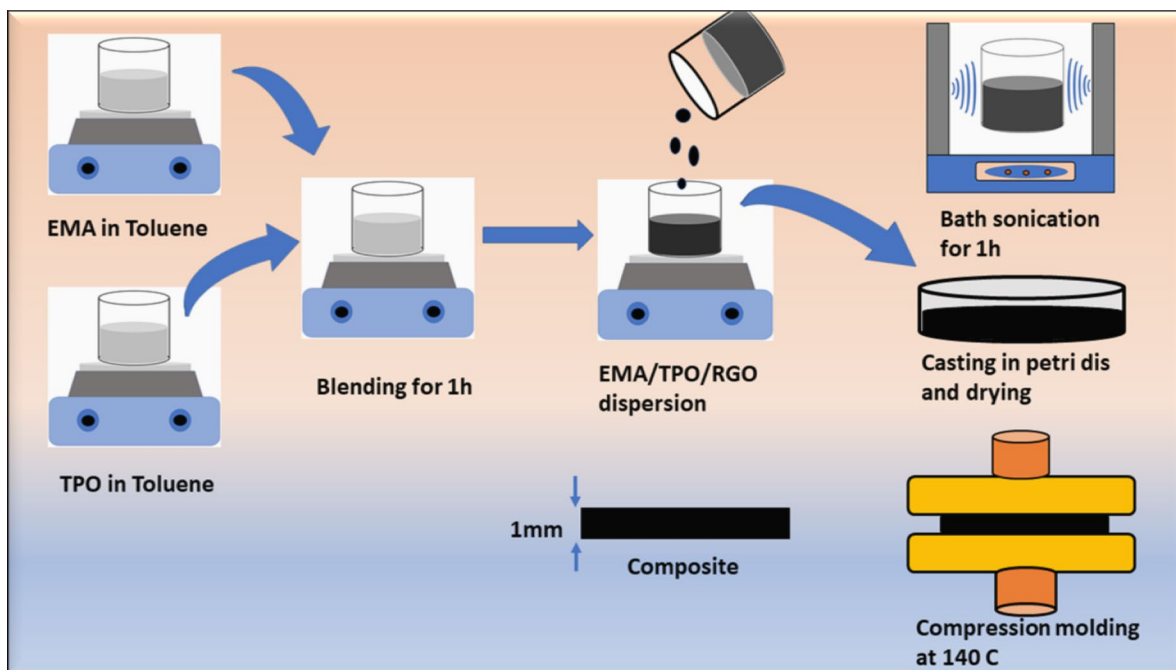


**Fig. 1** Process of blending for the creation of a composite involving EMA/TPO/RGO

## Characterization methods

The mechanical properties of EMA/TPO composites, both with and without the addition of RGO, were evaluated employing a Universal Tensile Machine (UTM) model Hounsfield H10 KS. The testing was conducted under standard atmospheric conditions. The tests were conducted in accordance with the parameters specified in ASTM D412-98, and a predefined crosshead speed of 500 mm per minute was utilised. The results were obtained by calculating the average of three test samples in the shape of dumbbells. The measurement of hardness was conducted utilizing a Shore A durometer, while wide-angle X-ray diffraction (XRD) analysis was carried out on both pure polymers and the resulting composites. The XRD analysis employed Ni-filtered Cu K radiation with a wavelength of 1.54 Å. The scanning rate employed for the experiment was 0.0050 (2/°), encompassing a  $2\theta$  angular span from  $10^\circ$  to  $65^\circ$ . The experimental measurements were carried out using an Xpert PRO instrument manufactured by PAN Analytical B.V., located in the Netherlands. The Fourier transform infrared (FTIR) spectroscopy technique was utilised in attenuated total reflection (ATR) mode to investigate the wavenumber range spanning from 4000 to  $400\text{ cm}^{-1}$  under ambient temperature conditions. The visualisation of polymer blend morphology and filler distribution in the various composites was facilitated by employing a Field Emission Scanning Electron Microscope (FESEM) with a 5 kV acceleration voltage (Merlin, Carl ZEISS Pvt Ltd.). The thermal response was evaluated using differential scanning calorimetry (DSC) using a Q2000 V24.10 instrument from TA Instruments, USA. The measurements were conducted in a nitrogen atmosphere throughout a temperature range of  $-80$  to  $150^\circ\text{C}$ , with a heating rate of  $10^\circ\text{C}/\text{min}$ . The results are shown in (Supplementary S1).

The thermal degradation temperature of the materials was evaluated using thermogravimetric analysis (TGA) with a Q5000 instrument from TA Instruments, USA. The samples had a weight range of 9 to 12 mg and were heated at a rate of  $20^\circ\text{C}/\text{s}$  up to a temperature of  $600^\circ\text{C}$  (Supplementary S3). The measurement of the DC conductivity of the polymer composites' electrical characteristics was conducted using a Keithley 6514 system electrometer.

$$\rho = t/AR \quad (1)$$

The equation was used to express electrical conductivity ( $\rho$ ) in terms of resistance ( $R$ ), thickness ( $t$ ), and sample area ( $A$ ). The AC impedance analyser (WinDETA Novotherm) was utilised to evaluate the AC conductivity within a frequency range of 10 Hz to 10 MHz while maintaining a voltage of 1 V. The electromagnetic interference (EMI) shielding effectiveness was calculated in the Ku band frequency range (14.5 to 20 GHz). This evaluation was conducted with a VNA model E5071C, MY46109484, manufactured by Agilent Technologies in the United States. The complex permittivity was derived from the scattering parameter by the utilisation of the Nicolson-Ross-Weir model. The thermal conductivity was evaluated using a TCi-3-A C-thermal analyser manufactured by Hot Disc (Canada).

## Result and discussion

### Analysis of RGO by XRD and Raman

Figure 2a illustrates the XRD spectra of the produced GO and RGO. The XRD evaluation of GO exhibited a distinct peak at a  $2\theta$  angle of  $10.81^\circ$ , providing evidence for the effective oxidisation of graphite finely powdered. Upon

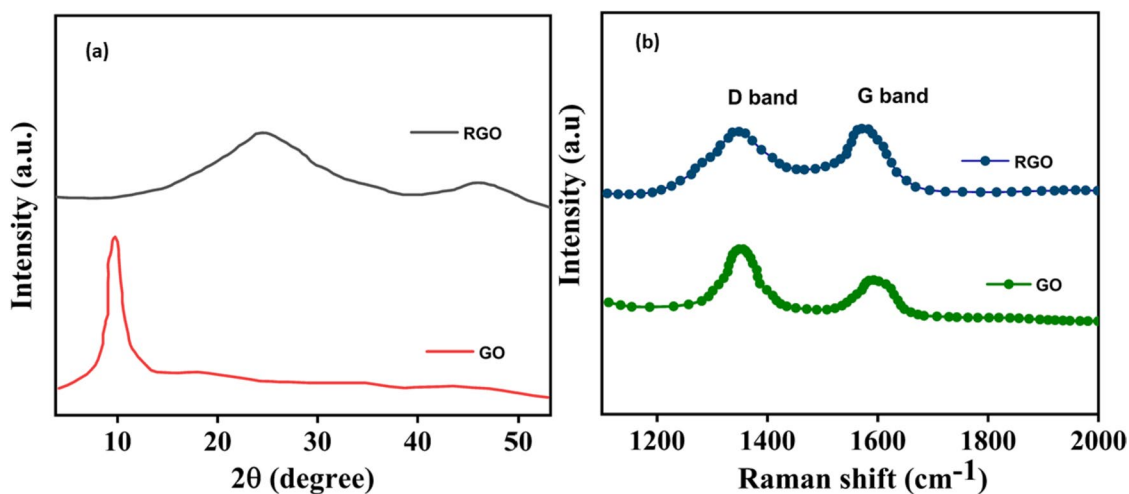


Fig. 2 The a XRD spectra b Raman spectra for both GO and RGO

reduction with hydrazine, GO underwent a transformation into RGO, evidenced by broad main peaks around  $24^\circ$  [16]. XRD analysis for blends and resulting composites with varying filler weights are depicted in Fig. (S2). It is worth mentioning that the polymer blend in its pristine state displayed a more pronounced peak, which suggests a decrease in crystallinity as a result of the blending process of the polymers. The inclusion of a 1 wt.% filler resulted in an augmentation of the peak intensity. This observation implies that when the filler loading is low, RGO functions as a nucleating agent, hence enhancing the degree of crystallinity. On the other hand, when the filler content is increased, the presence of RGO impedes the organised alignment of polymer chains, leading to a reduction in the degree of crystallinity within the blend system.

The Raman spectral analysis displayed in Fig. 2b verified the reduction of GO. The G-band elucidates the scattered arrangement of  $sp^2$  hybridised carbon atoms, while the D-band signifies structural flaws or disorder. The Raman spectra of graphene oxide (GO) exhibit two prominent bands, namely the D band and the G band, which are found at wavenumbers of  $1355\text{ cm}^{-1}$  and  $1600\text{ cm}^{-1}$ , correspondingly. These bands can be attributed to the presence of  $sp^3$  defects and in-plane vibrations of  $sp^2$  carbons in the GO structure. Significantly, the G band of reduced graphene oxide (RGO) exhibited a shift of about  $1600$  to  $1594\text{ cm}^{-1}$ , which suggests the inherent capability of RGO to remedy

hexagonal carbon-based flaws through a "self-healing" mechanism [16]. It is worth noting that the position of the D band in RGO remained unaltered.

In addition, the  $I_D/I_G$  ratios of GO and RGO were measured to be 0.94 and 1.02, respectively. The increased intensity ratio seen in RGO as compared to GO can be attributed to the generation of defects caused by the elimination of oxygen functional groups from the surface of GO. The increase in the intensity ratio between GO and RGO can be attributed to the decrease in the  $sp^2$  domain resulting from the conversion of GO to RGO. The Raman examination of blends and resultant composites with different filler weights is illustrated in Fig. S4.

## Mechanical properties

The experimental data for the tensile strength of the EMA/TPO/RGO composite, produced using varying weight proportions of RGO as a filler, are displayed in Fig. 3(a, b) and Table 1. The tensile strength of the pristine blend was measured at 7.6 MPa. Notably, the addition of 1, 3, 5, and 10 wt% RGO to the blend matrix led to an augmentation in tensile strength. However, when the composite reached a loading of over 10 wt% RGO, its tensile strength exhibited a decline. This decrease can be attributed to the blend system experiencing even dispersion of fillers at lower content levels, emphasising polymer-filler interactions. It aligns with theoretical

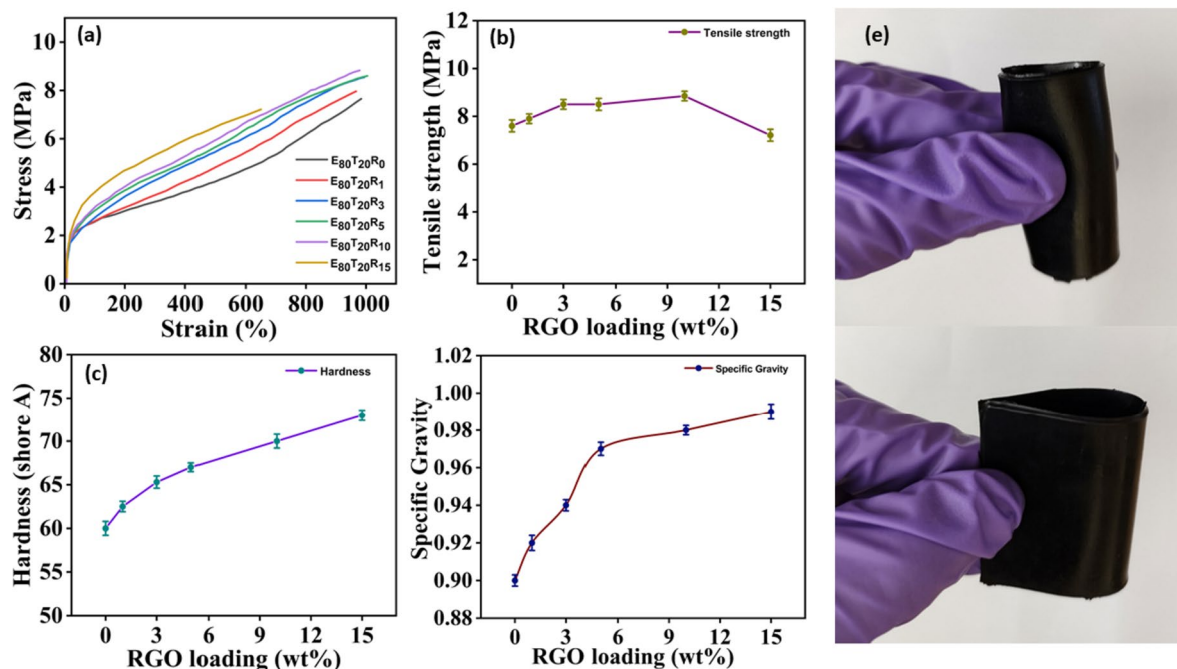


**Fig. 3** comprises several graphical representations: **a** the stress-strain profile of EMA/TPO/RGO composites, **b** the alteration in tensile strength, **c** the shifts in hardness, and **d** the changes in specific

gravity in response to escalating RGO loading. Additionally, **e** an image visually depicts the EMA/TPO/RGO composite 15 wt% RGO, showcasing its commendable flexibility.

**Table 1** Mechanical characteristics of EMA/TPO/RGO composite

Sample	T S (MPa)	Elongation @ break (%)	Modulus (100% elongation)	Modulus (200% elongation)	Modulus (300% elongation)
E <sub>80</sub> T <sub>20</sub> R <sub>0</sub>	7.6 ± 0.3	986 ± 30	2.5 ± 0.2	3.1 ± 0.3	3.4 ± 0.2
E <sub>80</sub> T <sub>20</sub> R <sub>1</sub>	7.9 ± 0.3	973 ± 32	2.5 ± 0.3	3.2 ± 0.2	3.7 ± 0.3
E <sub>80</sub> T <sub>20</sub> R <sub>3</sub>	8.5 ± 0.2	998 ± 40	2.8 ± 0.2	3.6 ± 0.4	4.3 ± 0.3
E <sub>80</sub> T <sub>20</sub> R <sub>5</sub>	8.6 ± 0.4	1005 ± 33	3.0 ± 0.4	3.7 ± 0.1	4.5 ± 0.2
E <sub>80</sub> T <sub>20</sub> R <sub>10</sub>	8.8 ± 0.3	980 ± 35	3.2 ± 0.3	3.9 ± 0.2	4.7 ± 0.1
E <sub>80</sub> T <sub>20</sub> R <sub>15</sub>	7.1 ± 0.2	653 ± 30	3.6 ± 0.2	4.6 ± 0.1	5.3 ± 0.2

expectations that incorporating higher filler content should increase tensile strength within polymer composites [21]. Nevertheless, an escalation in filler content triggers the accumulation of fillers and accentuates filler-filler interactions, resulting in a reduction in tensile strength. Figure 3(c) illustrates a progressive increase in the hardness of the polymer composite as filler content is raised. The specific gravity of the composite reaches 0.99 when incorporating a 15 wt% RGO content (as depicted in Fig. 3d). This specific gravity escalation follows the trend of rising filler percentage in the polymer blend. It's essential to note that flexibility plays an equally crucial role alongside enhanced tensile strength and hardness for practical applications. Figure 3(e) visually portrays the outstanding flexibility of the nanocomposite containing 15 wt% RGO.

### Wetting coefficient

Using the widely recognised Young's equation, an assessment of the wetting coefficient was conducted to ascertain the thermodynamic element that dictates the favoured integration of RGO within the immiscible EMA/TPO blend.

$$\omega_{12} = \frac{\gamma_{RGO/TPO} - \gamma_{RGO/EMA}}{\gamma_{TPO/EMA}} \quad (2)$$

Here, the terms  $\gamma_{RGO/TPO}$ ,  $\gamma_{RGO/EMA}$ , and  $\gamma_{TPO/EMA}$  represent the interfacial tensions between RGO and TPO, RGO and EMA, and TPO and EMA, respectively. The placement of RGO filler specifically occurs within the EMA phase of the EMA/TPO blend matrix when  $\omega_{12} > 1$ . The Owens, Wendt, Rebel, and Kaelble equation, which is widely used in both polar and non-polar systems, is utilised to assess the interfacial tension between two components.

$$\gamma_{12} = \gamma_1 + \gamma_2 - 2\sqrt{\gamma_1^d \gamma_2^d} - 2\sqrt{\gamma_1^p \gamma_2^p} \quad (3)$$

In this equation,  $d$  and  $p$  symbolise the dispersive and polar parameters of surface energy, respectively, while  $\gamma_1$  and  $\gamma_2$  denote the respective surface energies.

The determined free surface energy values for blend constituents (EMA and TPO) and RGO are listed in Table 2 [22–24], based on an analysis of existing literature. The

calculated  $\omega_{12}$  from Eq. (3) signifies a value of 2.39 for the EMA/TPO/RGO composite system. This observation indicates that the integration of reduced graphene oxide (RGO) tends to be mostly localised inside the polar ethylene methyl acrylate (EMA) phase of the blended system.

### Morphological study of EMA/TPO/RGO composite

The dispersion of the filler within the blended composite was examined using Field-Emission Scanning Electron Microscope (FESEM). Figure 4(a) presents the scanning electron microscopy (SEM) micrograph of RGO. The co-continuous morphology of the immiscible blend can be shown in Fig. 4(b), where the TPO phase was etch out through the use of cyclohexane. The co-continuous structure of this binary blend is evident, and the deliberate inclusion of RGO sheets into the ethylene–methyl acrylate (EMA) phase plays a significant role in facilitating the simultaneous occurrence of dual percolation in the resulting polymer composite. In addition, the SEM images of the cryo-fractured surface of composite samples containing different weight percentages of RGO are presented in Fig. 4(c–e). Figure 4(f) presents the TEM micrograph of RGO and the TEM micrograph of the EMA/TPO blend at 5 weight percent and 10 weight percent loading of the RGO component is shown in Fig. 4(g, h). Micrographs distinctly display two regions: a lighter, white region and a darker, black region. The EMA phase with agglomerated RGO filler content is depicted by the dark region, whereas no RGO filler in the TPO phase. The micrographs demonstrate that the RGO exhibited a preferential localisation inside particular regions, specifically the EMA Phase, within the polymer composite. This localisation was seen instead of a uniform distribution throughout the entire blend system.

**Table 2** Surface energy data of polymer and RGO

	$\gamma$ (mJ/m <sup>2</sup> )	$\gamma^d$	$\gamma^p$
TPO	32.8	31.3	1.5
EMA	42.8	38.9	3.9
RGO	46.7	4	42.7

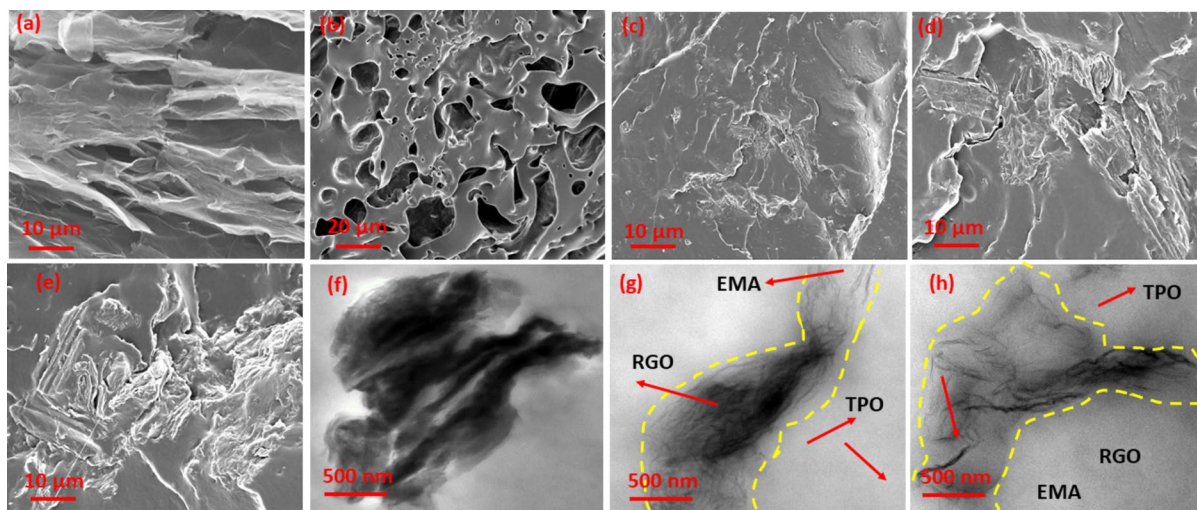


**Fig. 4** a FESEM micrograph of RGO, b FESEM micrograph of the EMA/TPO (80/20) blend (TPO was selectively etched out using cyclohexane), c-e further depict FESEM micrograph of the composite

with 5wt, 10wt, and 15wt RGO, respectively, f TEM micrograph of RGO g,h TEM micrograph of EMA/TPO/RGO composite

### Thermal conductivity of RGO-loaded EMA/TPO composite

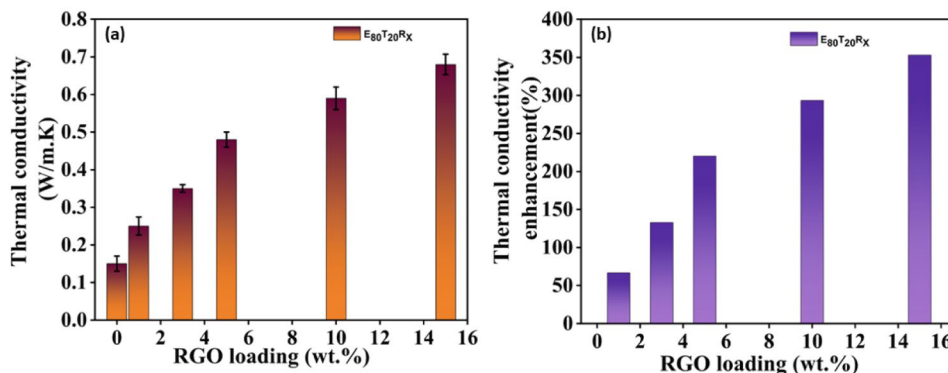
The thermal conductivity (T.C.) of the blend and its composites, incorporating varying weight percentages of RGO filler, can be assessed using the subsequent equation [25].

$$\eta = \frac{K_C - K_M}{K_M} \tag{4}$$

In this context,  $K_M$  represents the T.C. of the blend matrix, while  $K_C$  refers to the T.C. of the resulting composite. The T.C. values for the blend composites at room temperature are depicted in Fig. 5(a, b) for different loadings of RGO. The T.C. of the pure EMA/TPO blend is initially measured to be 0.16 W/mK. It is evident that the incorporation of RGO within the blend elevates its thermal conductivity. Specifically, the introduction of 1 wt% RGO enhances the composite's T.C. by 66%, reaching 0.25 W/

mK. Notably, a proportional relationship between RGO content and T.C. is observed, indicating the establishment of a network of thermally conductive RGO sheets. With a 3 wt% RGO addition, the EMA/TPO composite demonstrates a T.C. of 0.35 W/mK, marking a 2.33-fold increase. Impressively, the blend composite experiences a remarkable enhancement of T.C. by 3.5 times, reaching 0.48 W/mK, when supplemented with 5 wt% RGO. Upon adding 10 wt.% and 15 wt.% RGO, the EMA/TPO composite showcases notable T.C. values of 0.59 W/mK and 0.68 W/mK, respectively. Notably, the incorporation of 15 wt% RGO into the EMA/TPO matrix yields a substantial 353% escalation in T.C. compared to the neat blend. These results show that the well-known Joule heating effect is a highly efficient method for microwave energy dissipating in the EMA/TPO/RGO composite. The EMA/TPO/RGO composite as a result effectively dissipates heat energy, particularly during the emission of electromagnetic waves.

**Fig. 5** a Shows how the RGO loading affects the thermal conductivity. b Percentage increase in the T.C. with RGO content



## DC and AC conductivity

The electrical conductivity of the polymer composite is subject to various factors, including inherent conductivity, the distribution of fillers within the matrix, the type of fillers used, and the variables involved in the processing. Figure 6(a) depicts the relationship between the concentration of RGO and the direct current (DC) conductivity of the polymer composite. The polymer blend in its pure form demonstrates insulating characteristics, as seen by its direct current conductivity of  $10^{-11}$  S/cm. The incorporation of RGO leads to a significant enhancement in electrical conductivity, with a notable rise observed at an RGO loading of 15 wt%. Specifically, the electrical conductivity reaches a value of  $10^{-2}$  S/cm at this loading concentration. An increase in direct current (DC) conductivity is found when the weight percentage (wt%) of RGO is between 0 and 1 wt% in the blend matrix. This is followed by a substantial increase in conductivity between 1 and 3 wt% RGO, suggesting the presence of a percolation threshold within this range. After surpassing a filler concentration of 5 wt%, there is a minimal increase in electrical conductivity. This investigation reveals that the composite EMA/TPO/RGO has a percolation threshold ranging from 1 to 3 wt%. The power law equation

of classical percolation theory can be utilised to make predictions regarding the percolation threshold concentration.

$$\sigma_{DC} = \sigma_0 (P - P_C)^t \text{ for } P > P_C \quad (5)$$

Taking logarithm on both sides, we can write Eq. (5) as given below

$$\log \sigma_{DC} = \log \sigma_0 + t \log (P - P_C) \quad (6)$$

In this context, the variable  $P_C$  is used to represent the percolation threshold, while  $P$  symbolizes the filler percentage. The variable  $t$  is the critical exponent,  $\sigma_{DC}$  represents the DC conductivity, and  $\sigma_0$  is a constant. The determination of the value of  $t$ , which serves as a measure of the lattice distensibility of the filler, is of utmost importance. When the value of  $t$  is less than 1.5, the conductivity is attributed to the interaction between roughly spherical agglomerates. Conversely, when the value of  $t$  is less than 3, the conductivity is attributed to the behaviour of individual particles. The figure labelled as Fig. 6(a) illustrates the utilisation of a linear-log plot to ascertain the most suitable curve for  $P_C$  by examining the relationship between  $\sigma_{DC}$  and  $P - P_C$ . The obtained best-fit line demonstrates values of 2.92 for  $t$  and 1.6 for  $P_C$ . The obtained  $t$  value indicates that the conductivity is attributed to the interplay between individual RGO sheets.

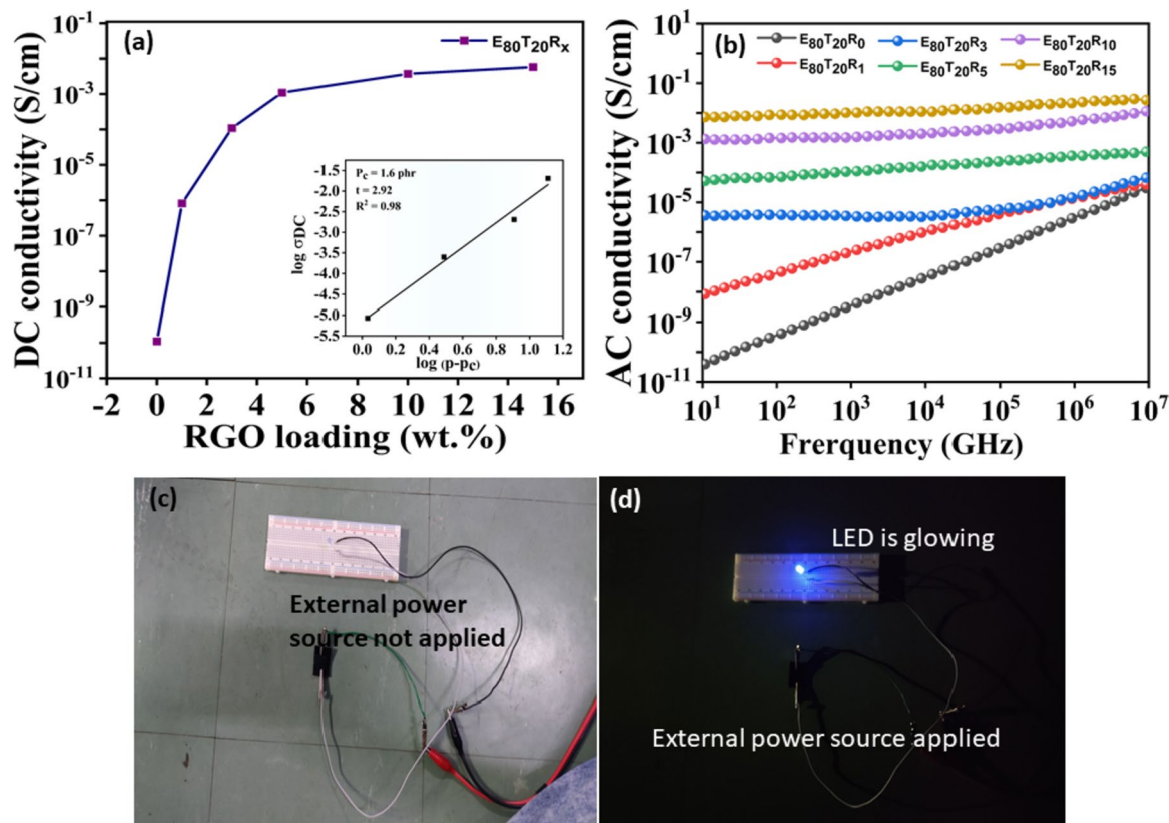


**Fig. 6** **a** direct current (DC) conductivity of the EMA/TPO blend and its composites, **b** the alternating current (AC) conductivity of EMA/TPO blend and their composites, **c**, **d** demonstration of EMA/TPO/RGO composite's electrical behaviour



Figure 6(b) illustrates the relationship between AC conductivity and frequency for both the blend and its composite with different filler loadings. The composite exhibits an increase in AC conductivity as the filler quantity is increased [26]. The alternating current (AC) conductivity of the polymer composite increases with frequency at lower concentrations of RGO filler. On the other hand, when the filler concentration is increased, the polymer composite demonstrates behaviour that is not dependent on frequency. Lower concentrations of RGO result in the isolation of individual RGO sheets. However, at greater concentrations, electrons can lead to their excitation and subsequent movement between conducting sites. This phenomenon establishes a more efficient electrically conductive network. Once the percolation threshold is surpassed, a network composed of interconnected RGO sheets is established within the polymer matrix. This network enhances the passage of electrons across conductive sites, leading to frequency-independent behaviour. In order to showcase the tangible electrical capabilities, a circuit is created utilising a light-emitting diode (LED) and a 5-V power supply, employing blend composites containing 15 weight percent RGO, as depicted in Fig. 6(c, d). The composites exhibit the emission of a vivid red LED light upon the connection of an external 5 V power supply. The nanocomposites exhibit good electromagnetic interference shielding performance due to the presence of a thick and interwoven reduced graphene oxide (RGO) network inside the mix matrix, which produces a beneficial interconnected conductive network interface.

### EMI shielding

The EMI shielding effectiveness (EMI-SE) is a logarithmic expression that quantifies the relationship between the power of incident electromagnetic (EM) radiation ( $P_i$ ) and the power of transmitted electromagnetic (EM) radiation ( $P_t$ ). Typically measured in decibels (dB), it reflects how shielding materials block energy. For instance, a material with a 20 dB EMI-SE can thwart nearly 99% of unwanted EM waves [27, 28]. The incident EM radiation power impacting shielding can be divided into reflected ( $R$ ), absorbed ( $A$ ), and transmitted ( $T$ ) power, where

$$A + T + R = 1 \quad (7)$$

In this investigation, a vector network analyser (VNA) gauged scattering parameters like  $S_{11}$ ,  $S_{21}$ ,  $S_{22}$ , which helped derive reflection ( $R=|S_{11}|^2$ ) and transmittance ( $T=|S_{21}|^2$ ) power coefficients, Absorbance ( $A$ ) was calculated using Eq. (8)

$$A = 1 - R - T \quad (8)$$

The cumulative shielding effectiveness ( $SE_T$ ) stems from absorption ( $SE_A$ ), reflection ( $SE_R$ ), absorption ( $SE_A$ ), and

internal multiple reflections ( $SE_M$ ) components, forming the overall effectiveness ( $SE_T$ ) [29, 30], written as

$$SE_T = SE_A + SE_R + SE_M \quad (9)$$

The occurrence of an impedance mismatch amongst different materials results in an increased level of reflection of electromagnetic waves. The presence of free electrons or charge carriers enables the process of microwave absorption. Factors like conductivity, permeability, and dielectric permittivity influence absorption. In practical scenarios, when the material thickness exceeds the skin depth or EMI  $SE_T$  surpasses 15 dB, EMI  $SE_M$  is negligible. Hence, EMI  $SE_A$  combines absorption and multiple reflections [31, 32], leading to

$$SE_T \approx SE_A + SE_R \quad (10)$$

The frequency-dependent  $SE_T$ ,  $SE_A$ , and  $SE_R$  of the manufactured composite were evaluated from the VNA using the following equations.

$$SE_T = 10\log_{10}\left(\frac{1}{|S_{12}|^2}\right) = 10\log_{10}\frac{1}{|S_{21}|^2} \quad (11)$$

$$SE_R = 10\log_{10}\left(\frac{1}{|S_{11}|^2}\right) \quad (12)$$

$$SE_A = 10\log_{10}\left(\frac{1 - |S_{11}|^2}{|S_{12}|^2}\right) \quad (13)$$

The reflection coefficient for forward waves is denoted as  $S_{11}$ , the forward transmission coefficient is indicated by  $S_{21}$ , and the reverse reflection coefficient is represented by  $S_{22}$ . Measurements of scattering parameters had been conducted in the expanded Ku-band frequency range, namely spanning from 14.5 to 20 GHz. Effective electromagnetic (EM) radiation shielding relies on electrical conductivity. Figure 7a illustrates the overall electromagnetic interference (EMI) shielding effectiveness ( $SE_T$ ) for created polymer composites. The pure EMA/TPO blend (80/20) exhibits -4 dB EMI SE, permitting easy passage of EM radiation. Adding conductive filler gradually enhances composite  $SE_T$  by constructing interconnected conductive pathways in the matrix, blocking EM radiation in polymer composites. Adding 15 wt% filler improves  $SE_T$  to -39 dB. Incorporating 3 wt% RGO in the blend system results in -23 dB EMI shielding efficiency, surpassing the -15 dB commercial use.

Figure 7(b, c) show  $SE_R$  and  $SE_A$  of the polymer composite. Figure 7d demonstrates that introducing RGO filler increases  $SE_A$  and  $SE_T$ . Notably,  $SE_A$  contributes more to  $SE_T$  than corresponding  $SE_R$ . This suggests that when conductive filler is added, absorption, rather than reflection, primarily attenuates

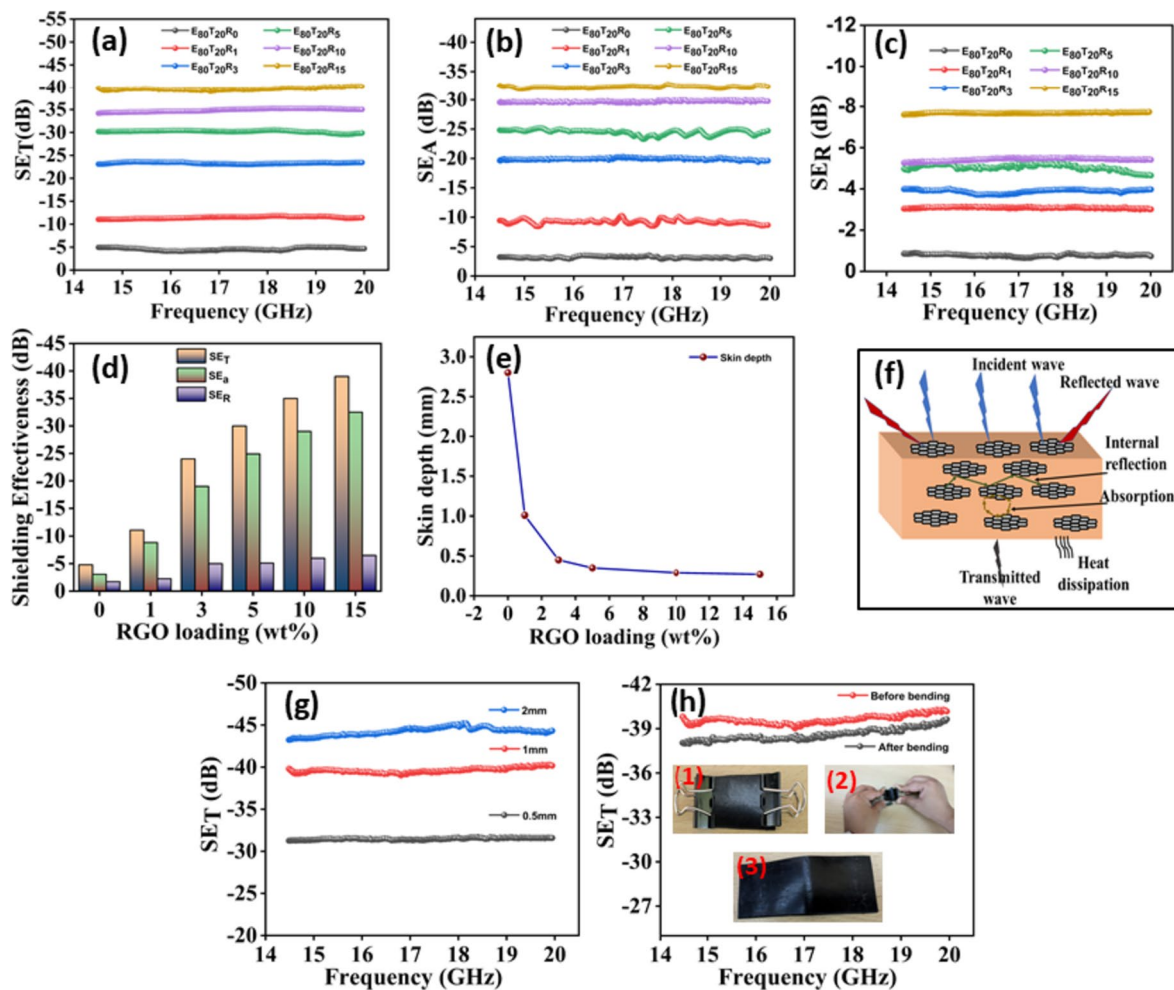


**Fig. 7** **a** Overall effectiveness of EMI shielding, **b**, **c** EMI shielding by absorption, reflection, respectively. **d**  $SE_T$ ,  $SE_R$  and  $SE_A$  at a fixed frequency (15 GHz). **e** Skin depth, **f** schematic for EMI shielding

mechanism, **g**  $SE_T$  of composite samples of 0.5, 1 and 2 mm thickness **h**  $SE_T$  before and after 300 bending of sample

advancing electromagnetic waves. Above the percolation threshold, a mesh-like structure emerges, potentially aiding EM absorption. A concentrated, continuous conductive structure formed above the percolation threshold allows smooth transmission of mobile charges and EM radiation absorption. Moreover, the presence of the RGO defect can serve as a site of polarization, leading to a decrease in the intensity of incident electromagnetic radiation by absorption. The electric dipole polarization in RGO flakes is a result of the presence of residual oxygen-containing groups such as C-O, -OH, and C=O. Nevertheless, the presence of mobile charge carriers in reduced graphene oxide (RGO) results in electron polarization, which is associated with dielectric loss. This phenomenon contributes to the attenuation of incident electromagnetic (EM) waves by facilitating absorption.

Since EM radiation affects surface-near composite materials due to radiation impact, skin depth ( $\delta$ ) also influences composite SE. The skin depth of a composite material refers

to the depth at which the strength of electromagnetic (EM) radiation decreases to  $1/e$  (about 36.8%) of the incident radiation. This concept is technically defined as

$$\delta = \frac{2}{\sqrt{f\mu\sigma}} = -8.68\left(\frac{t}{SE_A}\right) \quad (14)$$

Within the given framework, the variables  $t$ ,  $\mu$ ,  $\sigma$ , and  $f$  are utilized to symbolize the thickness of the sample, permittivity, electrical conductivity and frequency, respectively, measured in millimeters. Figure 7e depicts the alteration in skin depth with increasing filler concentration, while maintaining a constant frequency of 15 gigahertz. The graph depicts the relationship between the skin depth of composite materials and the incorporation of filler into the base polymer matrix. It demonstrates that as more filler is added over time, the composite materials exhibit an expanded network structure and improved

conductivity. The skin depth of the material is observed to be 0.26 mm when the loading of reduced graphene oxide (RGO) reaches 15 wt%. The aforementioned result suggests that the production of composites with the appropriate electromagnetic interference (EMI) shielding capabilities for practical applications can be achieved by decreasing the thickness of the sample and ensuring a suitable dispersion of filler materials. Figure 7f offers valuable insights into the mechanism of electromagnetic interference (EMI) shielding, highlighting the significant influence of the thickness of the shielding material in reducing the intensity of incoming electromagnetic radiation. Figure 7g illustrates the comprehensive electromagnetic interference (EMI) shielding efficiency (SE) of specimens with varying thicknesses (0.5 mm, 1 mm, and 2 mm) that incorporate 15 wt% reduced graphene oxide (RGO). It is worth noting that the electromagnetic interference (EMI) shielding effectiveness (SE) demonstrates an upward trend as the thickness of the sample increases. According to the data presented in Fig. 7g, it can be noticed that there is an increase in the overall shielding efficiency (SE) when the sample thickness is increased from 0.5 mm to 2 mm. Specifically, the total SE rises from -32.6 dB to -43 dB. Figure 7h showcases the total shielding efficiency before and after subjecting a 1 mm thick EMA/TPO composite with 15 wt% RGO content to 300 cycles of bending. Remarkably, there is only a marginal reduction in shielding efficiency following the bend test, highlighting the composite's effectiveness as a shielding material even under challenging dynamic conditions.

### Dielectric property

The investigation into the composite's ability to obstruct electromagnetic radiation relied on its dielectric properties. The Nicolson-Ross-Weir approach was employed, using "S" parameters ( $S_{11}$ ,  $S_{12}$ ), to assess the complex permittivity,

with the real and imaginary components being determined by the following Eq. (15):

$$\epsilon_r = \epsilon' + i_0\epsilon'' \tag{15}$$

The dielectric constant, also known as the real component of the complex permittivity, indicates the composite's ability to polarize and store electrical energy [33, 34]. On the other hand, the dielectric loss factor, which represents the imaginary component, is associated with the loss of electrical energy. Essentially, a higher magnitude of complex permittivity contributes to increased shielding efficiency through absorption mechanisms [35, 36]. Furthermore, Eq. (16) associates both the real and imaginary parts of the composites with specific capacitance (C), stimulated charge (Q'), and electric charge (Q).

$$\epsilon' = \frac{C}{C_0} = \frac{Q}{Q_0} = \frac{Q + Q'}{Q_0} \tag{16}$$

Figure 8(a-c) presents the frequency-dependent changes of the real and imaginary permittivity, as well as the  $\tan(\delta)$ , for the  $E_xT_xR_x$  composite within the frequency range of 14.5–20 GHz. Figure 8a demonstrates that an augmentation in the loading of reduced graphene oxide (RGO) results in an escalation of the real component of the complex permittivity of the composite. Figure 8b demonstrates a comparable pattern, wherein the imaginary component, which signifies the electric loss or energy dissipation of the composite, exhibits an upward trend as the RGO loadings grow.

Within the microwave frequency range, the real component of the complex permittivity is linked to interfacial polarization and space charge phenomena. The Maxwell–Wagner theory of polarization posits that in heterogeneous systems, the presence of interfaces between different media with distinct conductivity and permittivity leads to the development of virtual charges through interfacial polarization. The increase in the

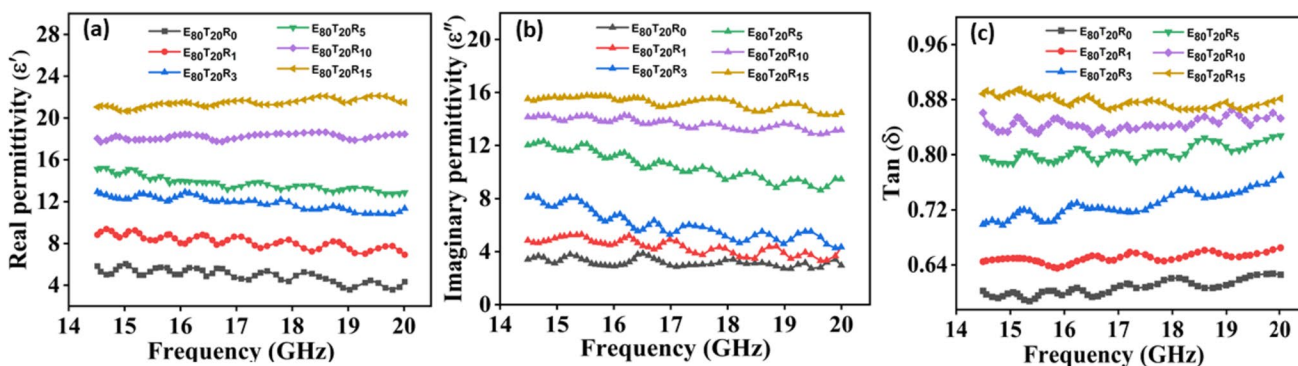
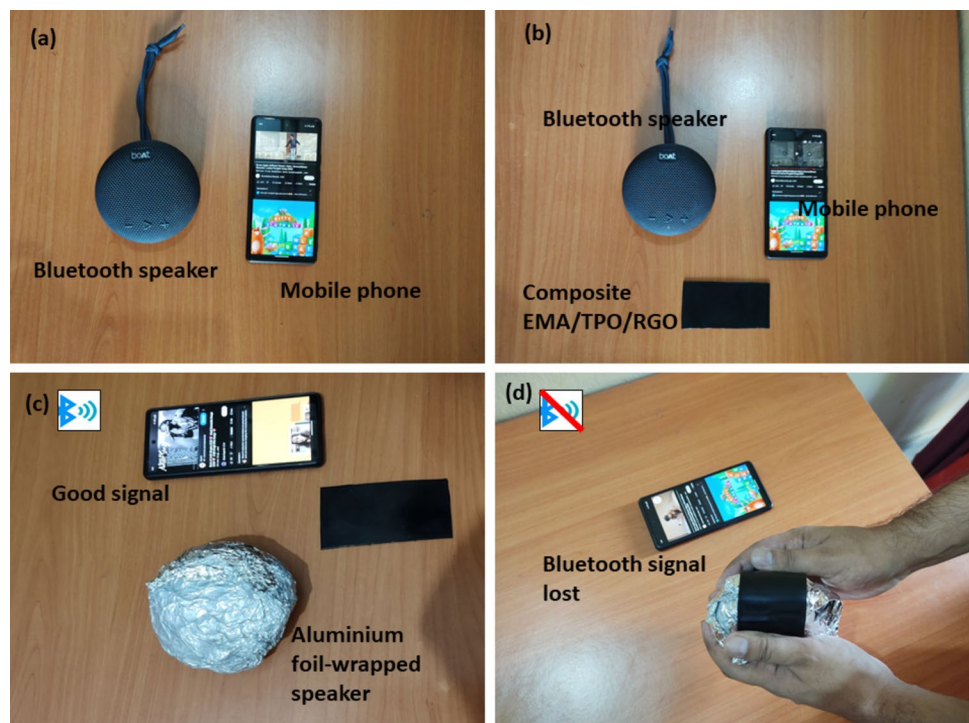


Fig. 8 Presents the variations of a the real component of the complex permittivity, b the imaginary component of the complex permittivity, and c the  $\tan(\delta)$  as a function of frequency

**Fig. 9** **a** The process of establishing a connection between a mobile phone and a Bluetooth speaker. **b** phone, Bluetooth speaker, EMA/TPO/RGO composite, while music is being played. **c** The smartphone is equipped with Bluetooth connectivity, allowing for the transmission of music to an audio system consisting of a Bluetooth speaker covered in aluminum foil, featuring a subtle grooved pattern. **e** The auditory output was not being produced by the Bluetooth speaker when the EMA/TPO/RGO composite was inserted into the narrow crevice



actual permittivity of the composite can be attributed to the emergence of micro capacitors inside the composite matrix. These micro-capacitors are formed by nanofiller particles or aggregates that function as electrodes while being surrounded by an insulating polymer. The advancement of micro-capacitors results in a rise in polarization centers, hence augmenting the actual permittivity with increasing RGO loadings. The existence of structural imperfections within the reduced graphene oxide (RGO) material adds to the creation of additional polarization centers, hence augmenting the actual permittivity of the composite. The imaginary permittivity of the composite material is also of significance in the context of electromagnetic interference (EMI) shielding applications. The value of ( $\epsilon''$ ) is influenced by the conductivity of the composite materials, which is determined by the existence of a three-dimensional conductive structure within the composites. The augmentation of RGO loadings leads to an increase in the quantity of three-dimensional networks within the composites, so resulting in a notable enhancement of their conductivity, as elucidated earlier. The conductivity of the composites is enhanced with higher RGO loading, resulting in a rise in dielectric loss. This phenomenon can facilitate the dissipation of electromagnetic waves. As a result, the increase in loading of reduced graphene oxide (RGO) in the blend system has a direct impact on enhancing the electromagnetic interference (EMI) shielding performance of the composite.

### Bluetooth demonstration

An experiment was done to showcase the practical utility of the nanocomposite. In the initial phase of the experiment, a musical signal was communicated from a mobile phone to a Bluetooth speaker, leading to the subsequent playback of the music by the speaker. Following that, we proceeded to completely encase the speaker with aluminium foil, while ensuring the presence of a small aperture in the foil to facilitate the transmission of the musical signal to the Bluetooth speaker. Subsequently, a segment of polymer composite was strategically placed onto the visible groove. Within this particular arrangement, the transmission of the auditory signal was impeded, resulting in the Bluetooth speaker being devoid of sound. The conducted experiment successfully demonstrated the efficacy of our synthesized nanocomposite material, which shares similarities with aluminium foil, in its ability to operate as both a conductive material and a shielding material, effectively blocking the signal. The complete experimental procedure is depicted in Video 1, while a concise overview is provided in Fig. 9(a-e).

### Conclusion

In the present study, a novel and economically efficient polymer blend composite reinforced with RGO has been effectively fabricated by the utilization of a solution mixing technique. The

composite material has a high level of effectiveness in shielding against electromagnetic interference. The increased tensile strength and modulus of the composite can be ascribed to the interaction between RGO and the blend matrix. The results of our Field-Emission Scanning Electron Microscopy (FESEM) investigation provide unambiguous evidence of the selective dispersion of RGO filler within the blend composite. The integration RGO nanosheets inside the polymer matrix facilitates the effective dissipation of heat from the composite material, leading to a significant thermal conductivity value of 0.75 W/K. In addition, the composite material demonstrates enhanced electrical conductivity and better dielectric permittivity, hence resulting in its superior efficacy for electromagnetic interference (EMI) shielding. By including a 15 weight percent of RGO into the composite material, a notable electromagnetic interference shielding effectiveness (EMI SE) of -39 dB was attained when the sample thickness was 1 mm. This study introduces a beneficial methodology for the fabrication of conductive EMA/TPO/RGO nanocomposites, which exhibit potential uses as shielding materials in diverse electronic devices.

**Supplementary Information** The online version contains supplementary material available at <https://doi.org/10.1007/s10965-023-03843-y>.

**Acknowledgements** Narayan Chandra Das expresses gratitude to the Science and Engineering Research Board (SERB), the Department of Science and Technology (DST), Government of India, for their kind provision of financial assistance, as awarded under Grant No. CRG/2021/003146. The authors express their gratitude for the extensive help and resources offered by the Indian Institute of Technology (IIT) Kharagpur.

**Funding** Science and Engineering Research Board (SERB), IN, CRG/2021/003146, Narayan Chandra Das.

**Data availability** All datas are available on request.

## Declarations

**Conflict of interest** We have no conflicts that need to be disclosed.

## References

- Anjana AC (2023) Dual role of magnetic ionic liquid in EMI absorbing polymer composites of P(VDF-TrFE) and f-MWCNTs. *J Polym Res* 30:130. <https://doi.org/10.1007/s10965-023-03460-9>
- Qin Q, Hu Y, Guo S et al (2023) PVDF-based composites for electromagnetic shielding application: a review. *J Polym Res* 30:180. <https://doi.org/10.1007/s10965-023-03506-y>
- Ankur K, Jasomati N, Narayan CD (2022) A journey of thermoplastic elastomer nanocomposites for electromagnetic shielding applications: from bench to transitional research. *Mater Adv* 3:2670–2691. <https://doi.org/10.1039/d1ma00989c>
- Ma L, Hamidinejad M, Zhao B et al (2022) Layered Foam/Film Polymer Nanocomposites with Highly Efficient EMI Shielding Properties and Ultralow Reflection. *Nanomicro Lett* 14:1–8. <https://doi.org/10.1007/s40820-021-00759-4>
- Haoran C, Pan Y, Qiang C et al (2021) Ultrathin flexible poly(vinylidene fluoride)/MXene/silver nanowire film with outstanding specific EMI shielding and high heat dissipation. *Adv Compos Hybrid Mater* 4:505–513. <https://doi.org/10.1007/s42114-021-00224-1>
- Tian K, Hu D, Wei Q et al (2023) Recent progress on multifunctional electromagnetic interference shielding polymer composites. *J Mater Sci Technol* 134:106–131. <https://doi.org/10.1016/j.jmst.2022.06.031>
- Rayar A, Naveen CS, Onkarappa HS et al (2023) EMI shielding applications of PANI-Ferrite nanocomposite materials: A review. *Synth Met* 295:117338. <https://doi.org/10.1016/j.synthmet.2023.117338>
- Pan D, Yang G, Abo-Dief HM et al (2022) Vertically Aligned Silicon Carbide Nanowires/Boron Nitride Cellulose Aerogel Networks Enhanced Thermal Conductivity and Electromagnetic Absorbing of Epoxy Composites. *Nanomicro Lett* 14:118. <https://doi.org/10.1007/s40820-022-00863-z>
- Junye C, Chuanbing L, Yingfei X et al (2022) Recent Advances in Design Strategies and Multifunctionality of Flexible Electromagnetic Interference Shielding Materials. *Nanomicro Lett* 14:80. <https://doi.org/10.1007/s40820-022-00823-7>
- Zhi X, Liu J, Bin ZH et al (2018) Simultaneous enhancements in electrical conductivity and toughness of selectively foamed polycarbonate/polystyrene/carbon nanotube microcellular foams. *Compos B Eng* 143:161–167. <https://doi.org/10.1016/j.compositesb.2018.01.022>
- Zhao H, Huang Y, Han Y et al (2022) Flexible and lightweight porous polyether sulfone/Cu composite film with bidirectional differential structure for electromagnetic interference shielding and heat conduction. *Chem Eng J* 440:135919. <https://doi.org/10.1016/j.cej.2022.135919>
- Jang D, Choi BH, Yoon HN et al (2022) Improved electromagnetic wave shielding capability of carbonyl iron powder-embedded lightweight CFRP composites. *Compos Struct* 286:115326. <https://doi.org/10.1016/j.compstruct.2022.115326>
- Yao B, Xu X, Li H et al (2021) Soft liquid-metal/elastomer foam with compression-adjustable thermal conductivity and electromagnetic interference shielding. *Chem Eng J* 410:128288. <https://doi.org/10.1016/j.cej.2020.128288>
- Govind KS, Nirmala RJ (2023) Flexible N-Doped Carbon Nanofiber-Polydimethylsiloxane Composite Containing La<sub>0.85</sub>Sr<sub>0.15</sub>CoO<sub>3-δ</sub> Nanoparticles for Green EMI Shielding. *ACS Appl Nano Mater* 6:6024–6035. <https://doi.org/10.1021/acsnm.3c00382>
- Poushali B, Sayan G, Tushar KD et al (2018) Superior electromagnetic interference shielding effectiveness and electro-mechanical properties of EMA-IRGO nanocomposites through the in-situ reduction of GO from melt blended EMA-GO composites. *Compos B Eng* 134:46–60. <https://doi.org/10.1016/j.compositesb.2017.09.046>
- Arunima D, Ranadip B, Sarbaranjan P et al (2020) Nanostructured cigarette wrapper encapsulated PDMS-RGO sandwiched composite for high performance EMI shielding applications. *Polym Eng Sci* 60:3056–3071. <https://doi.org/10.1002/pen.25536>
- Meng Y, Sharma S, Chung JS et al (2022) Enhanced electromagnetic interference shielding properties of immiscible polyblends with selective localization of reduced graphene oxide networks. *Polymers (Basel)* 14:967. <https://doi.org/10.3390/polym14050967>
- Ankur K, Palash D, Jasomati N et al (2023) Tailored distribution of 1D nanoparticles in co-continuous EMA/TPO flexible polymeric blends used as emerging materials for suppressing electromagnetic radiation. *J Phys Chem Solids* 179. <https://doi.org/10.1016/j.jpcs.2023.111395>
- Ma PC, Liu MY, Zhang H et al (2009) Enhanced electrical conductivity of nanocomposites containing hybrid fillers of carbon nanotubes and carbon black. *ACS Appl Mater Interfaces* 1:1090–1096. <https://doi.org/10.1021/am9000503>

20. Arief I, Biswas S, Bose S (2017) Graphene analogues as emerging materials for screening electromagnetic radiations. *Nano-Struct Nano-Objects* 11:94–101
21. Ankur K, Palash D, Sangit P et al (2023) Preferential localization of conductive filler in ethylene-co-methyl acrylate/thermoplastic polyolefin polymer blends to reduce percolation threshold and enhanced electromagnetic radiation shielding over K band region. *Polym Compos* 44:1603–1616. <https://doi.org/10.1002/pc.27191>
22. Berger EJ (1990) A method of determining the surface acidity of polymeric and metallic materials and its application to lap shear adhesion. *J Adhes Sci Technol* 4:373–391. <https://doi.org/10.1163/156856190X00360>
23. Della VC, Deimichei A, Riccò T (1998) A multiliquid approach to the surface free energy determination of flame-treated surfaces of rubber-toughened polypropylene. *J Adhes Sci Technol* 12:1141–1180. <https://doi.org/10.1163/156856198X00371>
24. Kol A, Kenig S, Naveh N (2020) Silane-Modified Graphene Oxide as a Compatibilizer and Reinforcing Nanoparticle for Immiscible PP/PA Blends. *Polym Eng Sci* 60:180–191. <https://doi.org/10.1002/pen.25271>
25. Palash D, Ankur K, Jasomati N et al (2023) Facile preparation of self-healable and recyclable multilayered graphene-based nanocomposites for electromagnetic interference shielding applications. *Colloids Surf A Physicochem Eng Asp* 676:132244. <https://doi.org/10.1016/j.colsurfa.2023.132244>
26. Krishnendu N, Suman KG, Palash D et al (2023) Fabrication of lightweight and biodegradable EMI shield films with selective distribution of 1D carbonaceous nanofiller into the co-continuous binary polymer matrix. *J Mater Sci: Mater Electron* 34:773. <https://doi.org/10.1007/s10854-023-10212-4>
27. Ma RY, Yi SQ, Li J et al (2023) Highly efficient electromagnetic interference shielding and superior mechanical performance of carbon nanotube/polydimethylsiloxane composite with interface-reinforced segregated structure. *Compos Sci Technol* 232:109874. <https://doi.org/10.1016/j.compscitech.2022.109874>
28. Krishnendu N, Suman KG, Ankur K et al (2022) Facile production of binary polymer/carbonic nanofiller-based biodegradable electromagnetic interference shield films with low electrical percolation threshold. *Polym Eng Sci* 62:3841–3857. <https://doi.org/10.1002/pen.26151>
29. Jyoti J, Chauhan GS, Yang S et al (2023) Stretchable and lightweight MWCNTs/TPU composites films with excellent electromagnetic interference shielding and dynamic mechanical properties. *J Polym Res* 30. <https://doi.org/10.1007/s10965-023-03690-x>
30. Suman K G, Tushar K D, Sayan G et al (2022) Carbon nanotubes and carbon nanofibers based co-continuous thermoplastic elastomeric blend composites for efficient microwave shielding and thermal management. *Compos Part A Appl Sci Manuf* 161. <https://doi.org/10.1016/j.compositesa.2022.107118>
31. dos Anjos EGR, Brazil TR, de Melo Morgado GF et al (2023) Influence of MWCNT aspect ratio on the rheological, electrical, electromagnetic shielding, and mechanical properties of polycarbonate melt mixed nanocomposites. *J Polym Res* 30. <https://doi.org/10.1007/s10965-023-03453-8>
32. Palash D, Ankur K, Kinsuk N, Das NC (2023) Recyclable and super-stretchable conductive elastomeric composites with a carbon nanostructure interconnected network structure for effective thermal management and excellent electromagnetic wave suppressor. *Polymer-Plastics Technol Mater* 62:889–908. <https://doi.org/10.1080/25740881.2023.2169160>
33. Palash D, Ankur K, Arijit J et al (2023) Super-Stretchable, Self-Healing 2D MXene-Based Composites for Thermal Management and Electromagnetic Shielding Applications. *ACS Appl Eng Mater* 1:1186–1200. <https://doi.org/10.1021/acsaenm.3c00016>
34. George G, Simon SM, Prakashan V et al (2018) Green and facile approach to prepare polypropylene/: In situ reduced graphene oxide nanocomposites with excellent electromagnetic interference shielding properties. *RSC Adv* 8:30412–30428. <https://doi.org/10.1039/c8ra05007d>
35. Palash D, Ankur K, Suman KG et al (2023) Self-healable and super-stretchable conductive elastomeric nanocomposites for efficient thermal management characteristics and electromagnetic interference shielding. *Synth Met* 294:117304. <https://doi.org/10.1016/j.synthmet.2023.117304>
36. Suman KG, Krishnendu SNC et al (2023) Combination effect of functionalized high aspect ratio carbonaceous nanofillers and carbon black on electrical, thermal conductivity, dielectric and EMI shielding behavior of co-continuous thermoplastic elastomeric blend composite films. *Chem Eng J Adv* 15:100505. <https://doi.org/10.1016/j.cej.2023.100505>

**Publisher's Note** Springer Nature remains neutral with regard to jurisdictional claims in published maps and institutional affiliations.

Springer Nature or its licensor (e.g. a society or other partner) holds exclusive rights to this article under a publishing agreement with the author(s) or other rightsholder(s); author self-archiving of the accepted manuscript version of this article is solely governed by the terms of such publishing agreement and applicable law.